A Satellite Study of the Atmospheric Forcing and Response to Moist Convection over Tropical and Subtropical Oceans

HIROHIKO MASUNAGA

Hydrospheric Atmospheric Research Center, Nagoya University, Nagoya, Japan

(Manuscript received 6 January 2011, in final form 13 June 2011)

ABSTRACT

Satellite data are analyzed to explore the thermodynamic evolution of tropical and subtropical atmospheres prior and subsequent to moist convection in order to offer an observational test bed for convective adjustment, which is central to the quasi-equilibrium hypothesis. Tropical Rainfall Measuring Mission (TRMM) and *Aqua* satellite measurements are projected onto a composite temporal sequence over an hourly to daily time scale by exploiting the temporal gap between the local satellite overpasses, which changes from one day to another. The atmospheric forcing and response to convection are investigated separately for deep convective and congestus clouds. In the deep tropics, systematic moisture transport from the atmospheric boundary layer (ABL) to the free troposphere is evident in association with deep convection. The quick ABL ventilation suggests a swift convective adjustment but is preceded by a steady buildup of ABL moisture, which does not imply continuous adjustment to equilibrium. The evolution of convective available potential energy (CAPE) is controlled not only by the ABL moisture but also largely by a coincident ABL cooling linked with a bipolar anomaly of tropospheric temperature. The ABL moisture and temperature effects together lead to a rapid drop of CAPE for 12 h preceding convection, followed by a restoring phase that emerges as the cool anomaly recovers for a day or two. When moist convection is brought by congestus clouds with no deep convection nearby, CAPE gently increases over a period of 1–2 days until congestus occurs and then declines as slowly, suggestive of no efficient convective adjustment. The subtropical atmosphere shows no sign of convective adjustment whether or not vigorous convection is present.

1. Introduction

Moist convection has been long known to be a critical element of tropical atmospheric dynamics. Enormous spatial and temporal gaps lying between convective cloud cells and atmospheric motions of interest, however, give rise to a challenge to the theories and modeling of the tropical atmosphere. A way to avoid this difficulty is to filter out individual cumulus clouds from large-scale dynamics, assuming that the neutralizing effect of a cloud ensemble works quickly against the large-scale forcing, slowly destabilizing the atmosphere. Arakawa and Schubert (1974) explored this idea and argued that a cumulus cloud ensemble may be considered to be in ''quasi equilibrium'' (QE) with large-scale forcings. The QE hypothesis has since been central to a school of cumulus parameterization (Arakawa 2004), and different versions of QE thinking form the basis for many theories and (semi)analytical modeling of tropical atmospheres (e.g., Emanuel et al. 1994; Neelin and Yu 1994; Raymond 1995; Emanuel 1995; Neelin and Zeng 2000).

While analyses of in situ sounding data generally support the QE assumption (Arakawa and Schubert 1974; Lord and Arakawa 1980; Lord 1982), it would be beneficial to extend the regional QE testing to the whole tropics beyond individual field campaigns representing relatively limited regions and periods of time. Brown and Bretherton (1997), analyzing monthly-mean global datasets of air temperature and surface humidity, showed that thermodynamic coupling between the atmospheric boundary layer (ABL) and free troposphere exists but is not as strong as predicted from the strict QE theory. Although the QE assumption is corroborated by recent work (e.g., Holloway and Neelin 2007), stochastic deviations from the QE state are also present in the satellite-observed moisture and temperature fields, suggesting the need for revisions to the QE hypothesis as originally postulated (Neelin et al. 2008).

Corresponding author address: Hirohiko Masunaga, Hydrospheric Atmospheric Research Center, Nagoya University, F3-1(200) Furocho Chikusa-ku, Nagoya 458-0015, Japan.
E-mail: masunaga@hyarc.nagoya-u.ac.jp

DOI: 10.1175/JAS-D-11-016.1

Efficient convective adjustment may not be expected where convective clouds do not develop deeply enough to penetrate the troposphere, as is the case for the subtropics under the influence of a strong trade inversion. The absence of deep convection, however, does not immediately mean the lack of convective processes that could alter large-scale atmospheric states. The QE assumption in its original form was relaxed to some degree by Raymond (1995) and Emanuel (1995) in ''boundary layer quasi-equilibrium,'' where no explicit constraint is imposed on free-tropospheric thermodynamics. Shallow cumulus and cumulus congestus, with cloud tops as low as 2–6 km, are widely observed across tropical and subtropical oceans (Johnson et al. 1999) and participate in tropical climate dynamics by ventilating the ABL and moistening the lower free troposphere (Yanai et al. 1973; Neggers et al. 2007). Growing observational evidence shows that the free-tropospheric moistening proceeds in phase with the gradual deepening of shallow cumulus from the developing through mature stages of the Madden–Julian oscillation (MJO) (Kemball-Cook and Weare 2001; Kikuchi and Takayabu 2004; Kiladis et al. 2005; Masunaga et al. 2006; Benedict and Randall 2007; Masunaga 2009; Katsumata et al. 2009). Some recent versions of QE theory incorporate the midtropospheric moisture control on the vertical structure of convective heating in the context of convectively coupled equatorial waves (Khouider and Majda 2006; Kuang 2008). The QE premise of instant convective adjustment has yet to be tested against observations when moist convection is dominated by shallow and congestus clouds.

A short but finite convective adjustment time τ_{cnv} has important implications for large-scale dynamics. A nonzero adjustment time is incorporated in versions of cumulus parameterization (Betts 1986; Moorthi and Suarez 1992; Zhang and McFarlane 1995), and the impacts of delayed convective response on large-scale dynamics have been theoretically explored (Emanuel 1993; Neelin and Yu 1994). While convective adjustment time is considered as typically an hour or two (Arakawa and Schubert 1974; Betts and Miller 1986), the mesoscale organization of convective clouds can further delay the convective response (Xu et al. 1992). Few observational studies, however, have paid full attention to the nature of convective adjustment itself. Existing studies observationally verifying the QE hypothesis are based on ''indirect'' testing where mean state temperature and humidity, with the variability over τ_{cnv} unresolved, are examined to see if they behave as expected from the QE hypothesis. The present work, in contrast, attempts to directly trace the evolution of atmospheric states changing over an hourly to daily time scale.

A technical challenge to such direct testing with global observations is the limited sampling frequency in satellite measurements. Low earth-orbiting (LEO) satellites revisit any given location only twice a day or even less frequently and thus are unable to resolve any event varying within half a day. Geostationary satellites, on the other hand, are excellent in fine temporal sampling but do not carry sensors capable of measuring air temperature or detecting precipitation beneath a cloud layer. In this study, an analysis method is devised to overcome this difficulty and statistically delineate how the atmosphere thermodynamically forces and responds to convective clouds over a short period of time.

The primary goals of this work are to 1) provide an observational test bed for convective adjustment based on global, long-term satellite measurements, 2) explore deep convective and congestus cloud interactions with large-scale atmospheric thermodynamics, and 3) investigate differences between deep tropical and subtropical atmospheres in their ways of interacting with moist convection. Sections 2 and 3 describe the datasets and analysis method, respectively, and the results are presented in section 4. The findings of this paper are summarized and discussed in section 5.

2. Data

The present analysis is based exclusively on satellite measurements. Deep convective and congestus clouds are each detected by the Tropical Rainfall Measuring Mission (TRMM) Precipitation Radar (PR) and Visible/Infrared Scanner (VIRS), while the vertical structure of air temperature and humidity are profiled by the *Aqua* Atmospheric Infrared Sounder (AIRS)/Advanced Microwave Sounder Unit (AMSU). Precipitation from the *Aqua* Advanced Microwave Scanning Radiometer for Earth Observing System (EOS) (AMSR-E) is also analyzed. Each data product is described to some detail in this section.

a. TRMM PR and VIRS

The TRMM satellite, launched in late 1997, is a sun-asynchronous satellite with the local overpass time drifting over a recurrence period of about 23 days (or 46 days if ascending and descending orbits are separated). The TRMM PR is a Ku-band (13.8-GHz) radar and the VIRS is an imager equipped with five channels from visible to infrared wavelengths (Kummerow et al. 1998). This study, following Masunaga et al. (2005) and Masunaga and Kummerow (2006), uses TRMM PR echo-top height and VIRS infrared (10.8 μm) brightness temperature T_b to identify congestus and more vigorous convection separately. The PR echo-top height is the maximum altitude

of detectable radar echo, where at least three consecutive bins are required to contain a reflectivity equal to or exceeding 19 dBZ. Simultaneous PR and VIRS measurements are matched on a 1/4° grid.

In this paper "congestus" is defined in its broad sense, consisting of both precipitating shallow cumulus (echo-top height < 4 km and $T_b > 260$ K) and cumulus congestus (echo-top height between 4 and 6 km and $T_b > 245$ K) as defined by Masunaga et al. (2005). Raining clouds that develop not much beyond the lower or mid-troposphere all fall into the congestus category in the current definition. Nonprecipitating clouds are not included because the TRMM PR is insensitive to cloud droplets. Deep convective clouds are delineated by echo-top heights higher than 4 km and T_b values colder than 245 K and potentially contain both organized convective systems (including stratiform rain areas with high cloud tops) and isolated cumulonimbi penetrating to the tropopause. Deep convection in the current definition corresponds to deep convective and deep stratiform systems combined together in the Masunaga et al. (2005) terminology.

b. Aqua *AIRS/AMSU unit*

The *Aqua* satellite has been operating since mid-2002 in a sun-synchronous orbit with the local overpass time bound between 0130 and 0145 and between 1330 and 1345 local time (LT). The *Aqua* AIRS is a hyperspectral infrared sounder measuring atmospheric gas profiles with an average RMSE, when used in tandem with the AMSU, of 1 K for tropospheric temperature and 20% for relative humidity near every 1 km in height (Aumann et al. 2003). The cloud contribution to infrared emission from a partially cloudy column is algorithmically cleared within a 3×3 array of AIRS pixels (Susskind et al. 2003, 2006). The AIRS/AMSU version 5 level-3 daily product is adopted in this work for examining the vertical structure of air temperature and humidity as well as column-integrated water vapor (CWV). This product is constructed by projecting quality-controlled level-2 estimates onto a $1° \times 1°$ global grid. Separate satellite overpasses are never averaged together anywhere on the grid, so these temperature and moisture estimates may be considered as virtually instantaneous observations.

The AIRS standard pressure levels are 1000, 925, 850, and 700 hPa for the lowest four levels, followed by every 100 hPa up to 300 hPa and every 50 hPa farther above to 100 hPa. Air temperature is given at each of these levels while vapor mixing ratio and relative humidity are defined as the layer mean within a pair of consecutive levels. Saturation equivalent potential temperature θ_e^* and virtual temperature are calculated at the standard levels. The layer-mean vapor mixing ratio is interpolated to the standard levels when applied to the virtual temperature estimate. Virtual temperature will be required later for computing convective available potential energy (CAPE; see section 3a). The vapor mixing ratio in the lowest layer (i.e., the 1000–925-hPa mean) is extrapolated down to the surface vapor mixing ratio $q_{v,s}$. The extrapolation is carried out using a simple mixed-layer model as described in appendix A. Surface equivalent potential temperature, $\theta_{e,s}$, and CAPE are calculated using $q_{v,s}$ along with surface air temperature and pressure as provided by the AIRS/AMSU product. The AIRS/AMSU unit is denoted simply as the AIRS in the remainder of the paper.

c. Aqua *AMSR-E*

The *Aqua* AMSR-E is a conically scanning microwave radiometer equipped with 12 channels at 6 frequencies ranging from 6.9 to 89 GHz. The AIRS and AMSR-E are onboard the same platform and make virtually simultaneous observations except for a minor temporal offset due to the difference in scan geometry. Precipitation estimate from the AMSR-E is provided in a daily gridded product constructed with the Goddard Profiling algorithm (GPROF) (Kummerow et al. 2001). AMSR-E precipitation, when composited against the TRMM (section 3b), is analyzed for the purpose of illustrating the development and decline of convective activity as a reference to the associated thermodynamic variation as observed by the AIRS. AMSR-E data collocated with an invalid AIRS measurement are excluded from the analysis so that the sampling uniformity is assured.

d. Study period and regions

All the datasets described above are collected for 88 months from September 2002 to December 2009. Both TRMM and *Aqua* observations are available during this period except for occasional interruptions due to temporary sensor shutoffs. Periods of time when PR, VIRS, or AIRS data are missing are excluded from the analysis. Eight study regions over tropical and subtropical oceans are of current interest as defined in Table 1 and Fig. 1. As shown in Table 1, three of these regions are collectively designated as the deep tropics and another three as the subtropics for later convenience. Section 4a provides the reasoning for the choice of deep tropical and subtropical regions.

All AIRS and AMSR-E parameters are analyzed on a "large-scale" grid of $1° \times 1°$ resolution, so that the atmospheric states analyzed represent horizontal means over a roughly 100×100 km^2 area. Each large-scale grid box therefore contains at most sixteen 1/4° gridded TRMM

TABLE 1. Study regions. Landmasses included in the specified longitude and latitude ranges, if any, are excluded. The frequency of deep convective and congestus occurrences is listed in the rightmost two columns. Congestus occurrence is counted only where no deep convection coexists, while the total (unconditional) occurrence is given in parenthesis for reference.

Region	Acronym	Longitudes	Latitudes	Deep (%)	Congestus (%)
Tropical western Pacific	TWP	140°E–180°	5°S–5°N	5.00	2.01 (2.68)
Tropical eastern Pacific	TEP	130°–90°W	0°–10°N	1.95	1.51 (1.88)
Tropical Indian Ocean	TIO	50°–90°E	5°S–5°N	3.10	1.62 (2.10)
Tropical Atlantic Ocean	TAO	50°–10°W	0°–10°N	2.85	1.73 (2.31)
Southeastern Pacific	SEP	120°–80°W	25°–15°S	0.09	0.61 (0.63)
Northeastern Pacific	NEP	160°–120°W	15°–25°N	0.32	0.52 (0.58)
Southeastern Atlantic Ocean	SAO	30°W–10°E	25°–15°S	0.07	0.47 (0.49)
Northeastern Atlantic Ocean	NAO	60°–20°W	15°–25°N	0.52	0.90 (0.99)
Deep tropics	—	TWP + TIO + TAO		3.64	1.79 (2.36)
Subtropics	—	SEP + NEP + SAO		0.16	0.53 (0.57)

measurements. The deep convective or congestus occurrence, reported at 1° × 1° pixels where one or more subgrid TRMM pixel(s) is identified as deep convection or congestus, defines the base point for the composite analysis described later in section 3b. Repeating the same analysis with a 3° × 3° large-scale grid leads to a reduction in the amplitude of atmospheric variability but does not qualitatively alter the results presented in this paper (not shown).

3. Analysis method

a. CAPE

CAPE is calculated from AIRS measurements as

$$\int_{\mathrm{LNB}}^{\mathrm{LFC}} (T_{v,p} - T_v) R_d \, d\ln p, \qquad (1)$$

where LFC and LNB stand for the levels of free convection and neutral buoyancy, p denotes pressure levels, R_d is the gas constant for dry air, and T_v and $T_{v,p}$ are the virtual temperature of ambient air and an undiluted ascending air parcel, respectively. Condensate loading and the latent heat from freezing are not taken into account, so that the current estimate of CAPE is a qualitative measure of conditional instability rather than the precise quantification of buoyancy. The level of free convection (LFC) is determined assuming that the air parcel originates from the surface. To fill in vertical gaps among the standard pressure levels, AIRS temperature and vapor mixing ratio (and thus T_v) are linearly interpolated to every 1 hPa across the standard levels. The parcel virtual temperature is also computed at the same 1-hPa resolution so that LFC and LNB are each determined at the interpolated levels where $T_{v,p}$ meets T_v. The vertical integration in (1) is then carried out numerically by 1-hPa intervals to obtain CAPE. In a conditionally stable atmosphere where LFC is indefinable, CAPE is set to zero.

CAPE estimated for an undiluted air parcel is only an idealized measure of instability since the entrainment of dry free-tropospheric air could substantially reduce CAPE (Zhang 2009). Nevertheless, CAPE for an undiluted air parcel would remain useful in a qualitative sense unless the entrainment rate systematically varies with time to the extent that the reduced buoyancy due to entrainment completely alters the overall evolution of undiluted CAPE over a time scale of present interest. The potential effect of entrainment on the main conclusions of this work would need to be carefully examined in a future investigation.

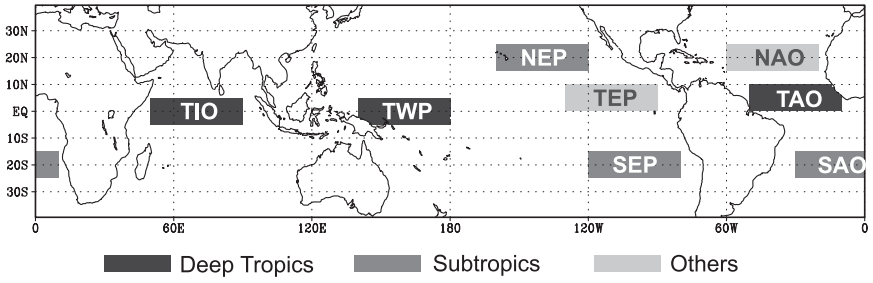

FIG. 1. Study regions. See Table 1 for acronyms.

b. Composite analysis

A main interest of the current work lies in the temporal evolution of large-scale atmospheric states associated with the development of deep convective and congestus clouds. Although the orbital configuration of LEO satellites makes it difficult to continuously monitor quickly changing atmospheres, the temporal sampling issue may be circumvented statistically by compositing a large number of snapshots in the way described as follows.

On a day when the TRMM happens to observe deep convection at a certain location, the *Aqua* satellite overpasses the same location some hours earlier or later than the TRMM observation. This time difference between TRMM and *Aqua* observations varies from one day to another since the local overpass time drifts over time for the TRMM whereas it is fixed for the *Aqua* (Fig. 2a). Every time when the TRMM detects deep convection, AIRS overpasses at that location are sought within ±120-h window and are time stamped. AIRS temperature and humidity profiles collected in this way are accumulated over a long period of time (>7 yr) and then averaged together at every hour of the TRMM–*Aqua* time difference. This procedure yields a continuous composite sequence as a function of time elapsed before and after the deep convective development (Fig. 2b). For temperature and humidity anomalies computed in the composite space, the background field is defined as the temporal average over the first and last 24 h combined (i.e., $-120 \le t \le -97$ h and $+97 \le t \le +120$ h). The *t* test is applied to the composite anomaly fields against the null hypothesis that finite anomaly is absent, and only statistically significant data exceeding the 95% level are plotted. Errors in the composite space are analyzed in appendix B.

The same technique applies also to congestus by compositing AIRS observations with respect to TRMM-detected congestus unaccompanied by deep convection. This additional constraint to preclude deep convection, unlike the deep convective case where no extra restriction is imposed, is aimed at isolating the contribution of congestus from that of coexisting deep convection. Deep convection is often surrounded by congestus clouds in mature convective systems, so that active deep convection, if not screened out, could largely dominate the congestus effect. The rightmost two columns in Table 1 imply that deep convection exists nearby for 20%–25% of the time when congestus is observed in the deep tropics. This percentage is much smaller in the subtropics.

Given that the satellite overpass time is confined within ±7 min around 0137 LT for *Aqua* and is accurately measured on an instantaneous basis for the TRMM, the composite time series may capture hour-to-hour changes in air temperature and humidity as well as day-to-day variability. This high temporal resolution is a unique advantage of utilizing multiple satellites together and effectively bypasses the limitations of individual satellites. Some previous studies have explored similar analysis techniques, combining an LEO satellite with geostationary or multisatellite infrared data (Kondo et al. 2006; Mapes et al. 2009) or with a 3-hourly global rainfall dataset (Zelinka and Hartmann 2009). The current strategy, focusing on two LEO satellites with different orbital configurations, fully exploits the capability of state-of-the-art LEO instruments such as the PR and AIRS. The composite time series is potentially smeared over a time of convective system life cycle, but in practice this does not limit the utility of the analysis as will be discussed in section 4b.

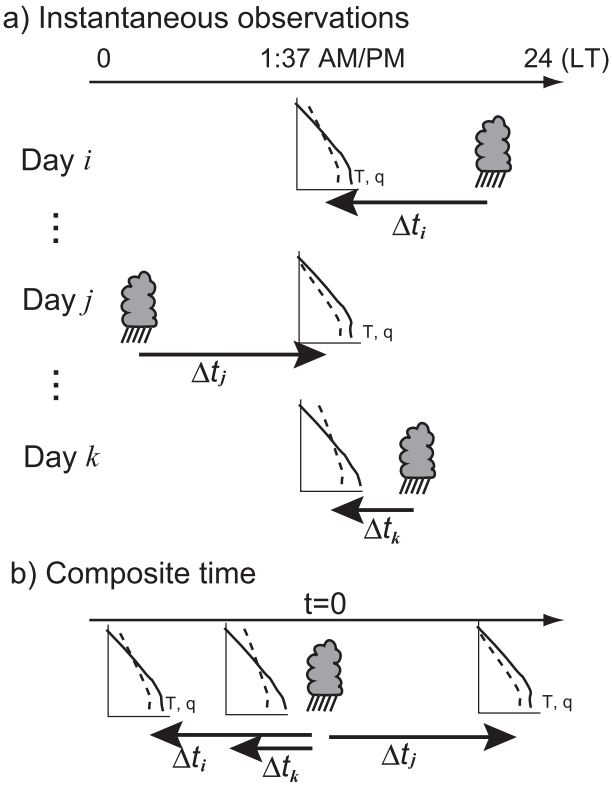

FIG. 2. A schematic outlining the composite analysis. (a) TRMM and *Aqua* observations on individual days. (b) The same observations projected onto the composite plot.

4. Results

Analysis results are presented in this section. The regional climatology of atmospheric states is examined first, and findings from the composite analysis follow next.

a. Regional climatology

The study regions listed in Table 1 are chosen to represent typical climate regimes over tropical and subtropical

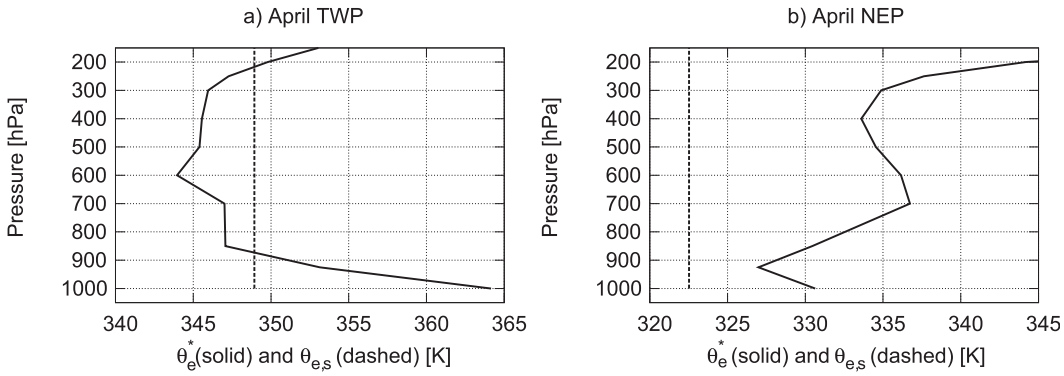

FIG. 3. The April climatologies of θ_e^* (solid) and $\theta_{e,s}$ (dashed) for selected regions: (a) tropical western Pacific and (b) northeastern Pacific.

oceans. The regional thermodynamic characteristics of the atmosphere are differentiated in terms of a combination of $\theta_{e,s}$ and θ_e^*. Two contrasting examples are shown in Fig. 3. In the tropical western Pacific (TWP; Fig. 3a), the domain with $\theta_e^* < \theta_{e,s}$ in the middle troposphere indicates that the atmosphere is conditionally unstable, or possibly virtually neutral (Xu and Emanuel 1989), as is typical of the deep tropics. On the other hand, θ_e^* stays higher than $\theta_{e,s}$ particularly above 900 hPa in the northeastern Pacific (NEP; Fig. 3b), suggestive of a stable condition where the ABL is capped by the trade inversion as is often the case over subtropical oceans.

Figure 4 plots $\theta_{e,s} - \theta_e^*$ as a rough measure of buoyancy for all the eight study regions and four separate months. The thermodynamic characteristics are quite separable at least for January and April, where TWP and the tropical Indian Ocean (TIO), tropical Atlantic (TAO), and tropical eastern Pacific (TEP) are found to

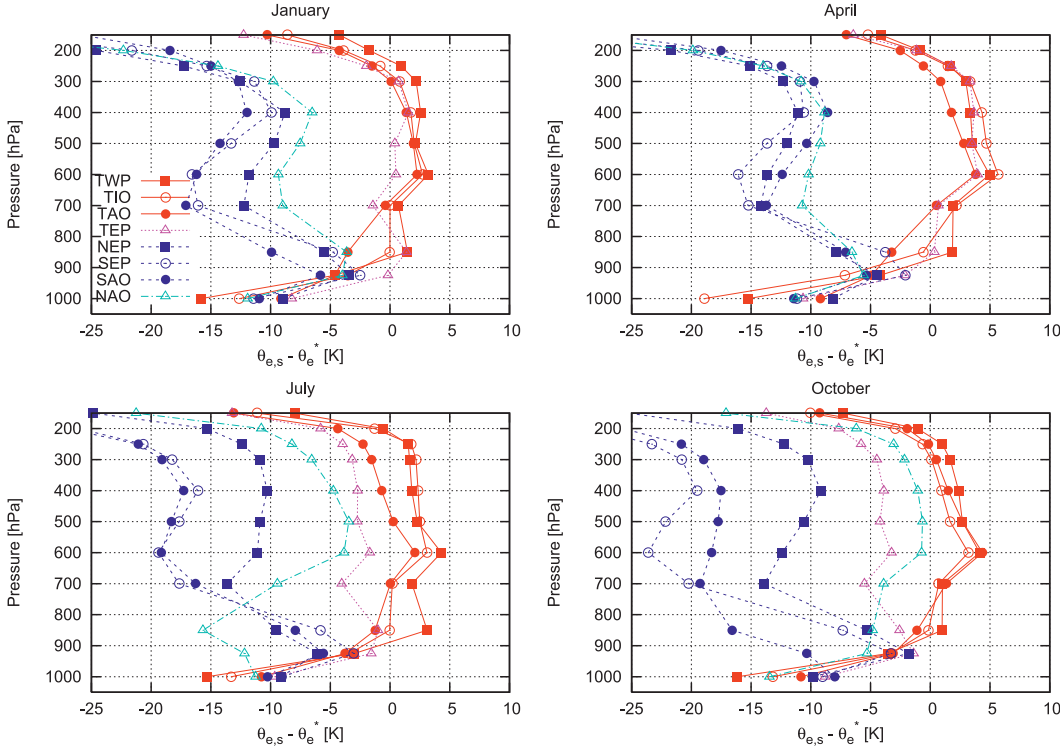

FIG. 4. Monthly climatologies of $\theta_{e,s} - \theta_e^*$ for all the study regions: (top left) January, (top right) April, (bottom left) July, and (bottom right) October. Different lines indicate different regions as labeled in (a) and are highlighted in red for the deep tropics, in blue for the subtropics, and in light red/blue for others.

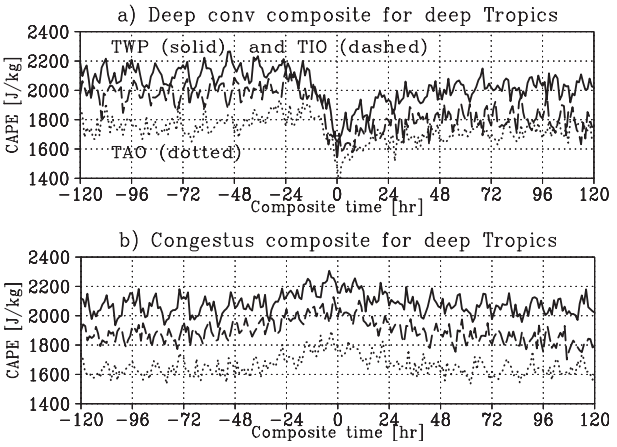

FIG. 5. The temporal sequence of CAPE in deep tropical regions composited with respect to (a) deep convective clouds and (b) congestus clouds. Different lines show different regions as labeled in (a).

be conditionally unstable and the other four regions stay stable. Table 1 indicates a close tie between dominant cloud types and stability; that is, deep convection predominates over congestus in the frequency of occurrence for the conditionally unstable regions while the inequality reverses for the stable areas. This regional contrast remains through the rest of the year except for TEP and the northeastern Atlantic Ocean (NAO), each of which migrates toward a more neutral or weakly stable state during July and October. These two regions with overwhelming seasonality are not analyzed in the remainder of the paper. The other six regions are seasonally consistent and may be safely considered as either deep tropical or subtropical representatives: TWP, TIO, and TAO for the deep tropics and NEP, the southeastern Pacific (SEP), and southeastern Atlantic Ocean (SAO) for the subtropics. The deep tropical regions are investigated first.

b. Deep tropics composite

Figure 5a shows the composite temporal sequence of CAPE over ±120 h around the deep convective occurrence for the three deep tropical regions. CAPE varies in magnitude from one region to another, with TWP highest and TAO lowest, but is consistent in the way it changes with time. CAPE stays nearly constant, aside from noisy fluctuations, until about a half day before the deep convective development ($t \approx -12$ h) when CAPE begins to drop sharply by 400–500 J kg^{-1} to the minimum at $t = 0$. Then CAPE is gently restored as time proceeds to a level slightly lower than it initially was. When composited with respect to congestus (Fig. 5b), in contrast, CAPE gradually increases with time by a modest amount (~200 J kg^{-1}) toward $t = 0$ and then slowly declines back to the original level. The increase and decrease in CAPE each take a day or two to complete. Note that deep tropical sounding is unstable most of the time and therefore a vast majority of individual soundings sampled for the composite plot have a finite CAPE. The effect of stable soundings (i.e., zero CAPE) on the composite CAPE will be discussed later in section 4d in comparison with the subtropical composite analysis.

To isolate key processes responsible for these contrasting behaviors of CAPE, humidity and air temperature projected into the composite space are investigated. The three deep tropical regions are combined together from now on, since the evolution of CAPE is found to be coherent across the regions studied. Figure 6 shows the composite moisture profile. The relative humidity anomaly systematically varies with time when composited with respect to deep convection (Fig. 6a). The whole free troposphere moistens toward the peak of deep convection ($t = 0$) and subsequently dries at a slower pace, not precisely in phase across different altitudes. The relative humidity anomaly is largest in the lower free troposphere (800–700 hPa) right at and slightly prior to the deep convective occurrence, immediately followed by a prominent upper-tropospheric humidity maximum at 400–300 hPa lingering for a day or two. Mapes et al. (2006) and Zelinka and Hartmann (2009) found a very similar feature in their analyses and attributed it to the presence of highly organized convective systems. The deepening of moist air associated with convective development is visible in vapor mixing ratio anomaly as well (Fig. 6b). The peak in vapor mixing ratio stays relatively low in altitude compared to the relative humidity field, suggesting that the upper-tropospheric relative humidity maximum should be partly owing to the upward decrease of tropospheric temperature and thus of the saturation vapor mixing ratio. The vapor mixing ratio anomaly clearly captures an ABL drying immediately after convection.

Surface vapor mixing ratio (blue in Fig. 6c) gradually increases with time until it abruptly drops at $t = 0$, while column water vapor (red in Fig. 6c) does not fall off as swiftly as $q_{v,s}$ but only slowly declines. These results together imply the quick ventilation of ABL moisture and a compensating free-tropospheric moistening (i.e., the vertical moisture transport from the ABL to the free troposphere associated with deep convection). The ABL ventilation time scale as inferred from the dropoff in $q_{v,s}$ reads no more than a few hours, comparable to the conventional estimate of τ_{cnv}. The ABL ventilation therefore may be thought of as a result of ''convective adjustment'' although a continuous adjustment to equilibrium appears to be hampered by the preceding buildup of ABL moisture.

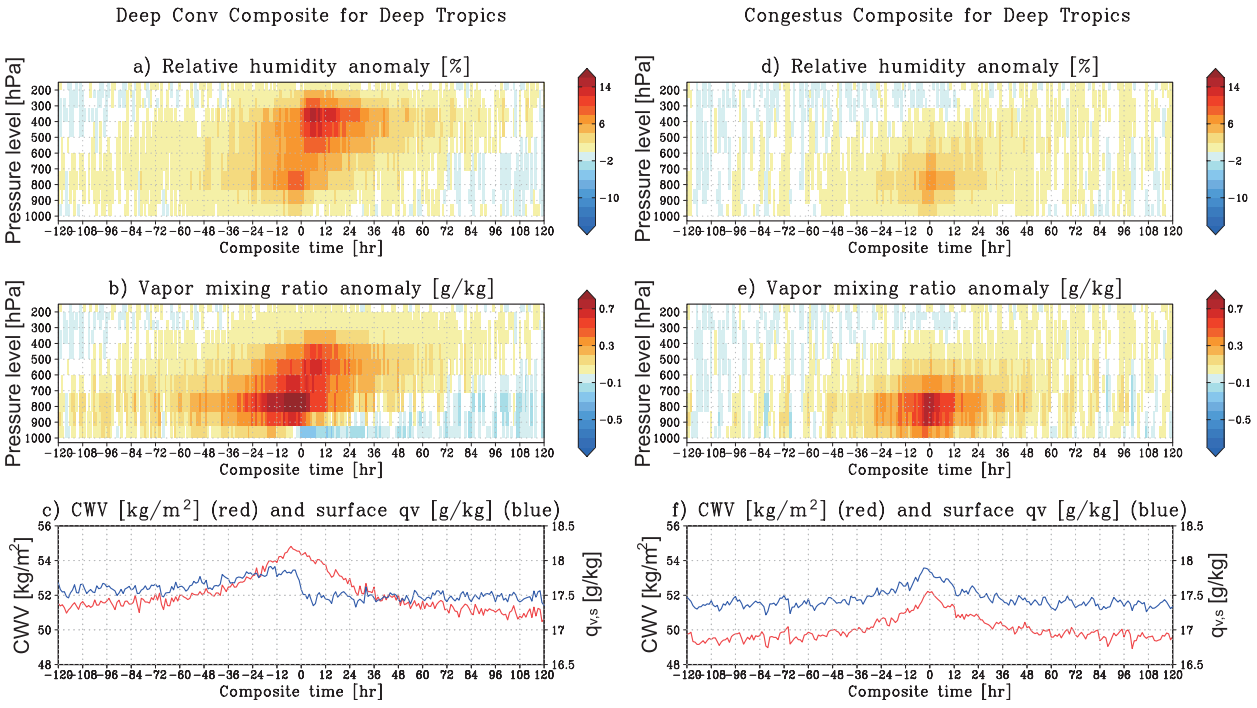

FIG. 6. The temporal sequence of (a) relative humidity anomaly (%), (b) vapor mixing ratio anomaly (g kg^{-1}), and (c) column water vapor (kg m^{-2}; red, labeled on the left axis) and surface vapor mixing ratio (g kg^{-1}; blue, labeled on the right axis), all composited with respect to deep tropical deep convection. The background level against which the anomaly field is defined in (a) and (b) is the temporal average over the first and last 24 h combined. Domains with statistical significance levels lower than 95% are blanked out in (a) and (b). (d)–f) As in (a)–(c), but composited with respect to deep tropical congestus.

When composited with respect to congestus (Figs. 6d,e), the moist anomaly is mostly confined to the lower free troposphere with no sign of upper-tropospheric moistening as found in association with deep convection. The temporal change of CWV associated with congestus is qualitatively very similar to the deep convective case, whereas $q_{v,s}$ exhibits no sharp drop at $t = 0$ but varies quite in phase with CWV. It follows that isolated congestus alone has a relatively limited capability of ABL ventilation and free-tropospheric moistening.

We can infer from the potential temperature difference or $\theta_{e,s} - \theta_e^*$ (cf. Fig. 4) that the atmosphere remains conditionally unstable throughout the 240-h sequence (Figs. 7a,d). The temperature anomaly field in the deep convection composite (Fig. 7b), on the other hand, shows a notable variation with time. A cool anomaly develops in the lower troposphere from a half day before the convection through a day or two after, accompanied almost 180° out of phase by a warm anomaly in the mid to upper troposphere. A similar bipolar structure (with a minor third pole near the tropopause) in temperature anomaly has been documented in the literature to appear in association with mesoscale convective systems (Sherwood and Wahrlich 1999; Mapes et al. 2006) and easterly waves (Reed and Recker 1971). The evolution of CAPE exhibits, as we have seen in Fig. 5, a rapid falloff and a slow restoration with the minimum in between at $t = 0$ (red in Fig. 7c). CAPE eventually settles at 1800–1900 J kg^{-1}, slightly lower than the initial level of 1900–2000 J kg^{-1}. The t test reveals that the difference between the initial and final CAPEs, when averaged over 24 h at each end, is statistically significant (>99%) in the deep tropical deep convective case. This dissipation of CAPE might be considered as the net effect of deep convection on large-scale atmospheric thermodynamics.

Composite rainfall sharply rises from $t = -12$ through 0 h, nearly in synchronization with the drop of CAPE, and then suddenly falls to the background level of about 2 mm day^{-1} (blue in Fig. 7c). The composite rainfall peak could be smeared to the degree imposed by the lifetime of convective systems, since the current compositing technique does not pinpoint the peak or any particular stage of the convective life cycle. Although this could challenge the performance of the composite analysis, the sharp cutoff in composite rainfall at $t = 0$ appears to suggest that the current analysis has the ability to capture changes as brief as a few hours when

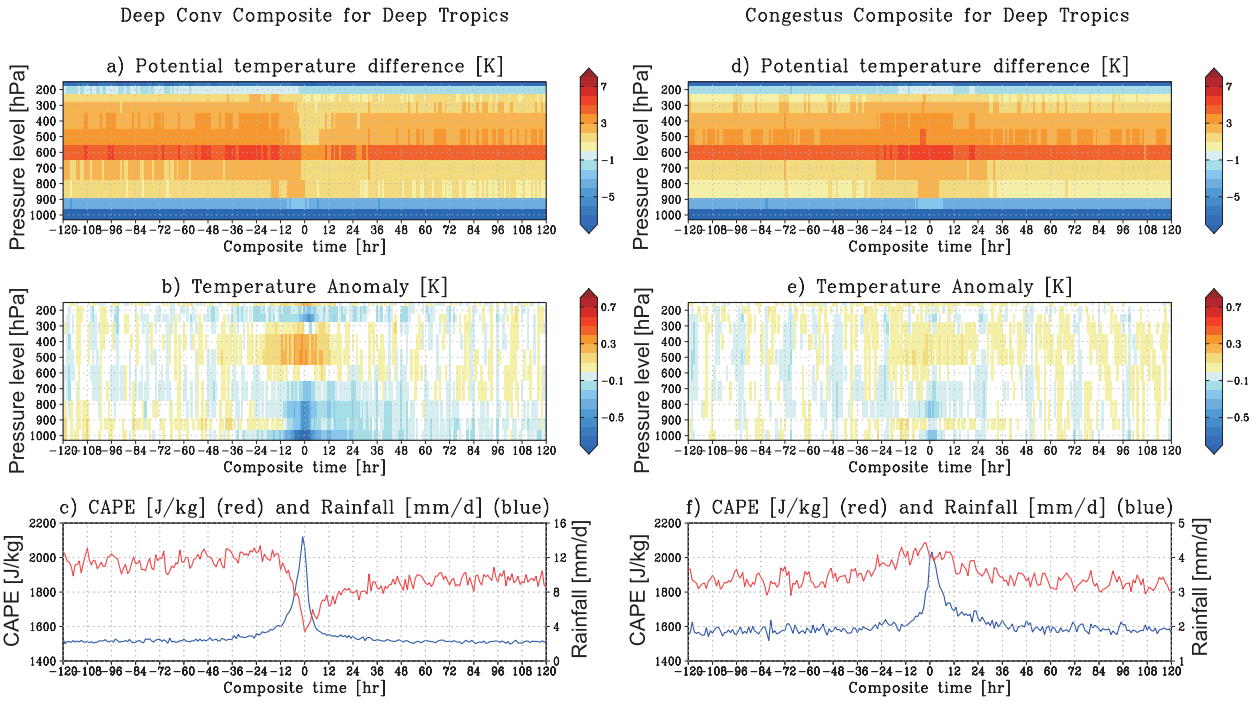

FIG. 7. The temporal sequence of (a) $\theta_{e,s} - \theta_e^*$ (K), (b) air temperature anomaly (K), and (c) CAPE (J kg^{-1}; (red, labeled on the left axis) and rainfall rate (mm day^{-1}; blue, labeled on the right axis), all composited with respect to deep tropical deep convection. Domains with statistical significance levels lower than 95% are blanked out in (b). (d)–(f) As in (a)–(c), but composited with respect to deep tropical congestus.

they occur. The peak value of about 15 mm day^{-1} would be even higher if all AMSR-E pixels were included without being screened where AIRS estimates are missing, since heavily raining grid boxes are often devoid of AIRS measurements (see appendix B). It should be noted, therefore, that the composite plots from the current analysis somewhat underrepresent the actual variability because of this sampling bias. The rainfall peak is about 4 mm day^{-1} in the congestus composite. No thermodynamic parameters, including $q_{v,s}$ and CAPE, vary as quickly as congestus rainfall, suggesting that the evolution of thermodynamic state is driven primarily by dry processes for congestus.

c. *Factors controlling CAPE*

It has been seen that CAPE has a restoring phase following the rapid decay concurrent with the deep convective development. Individual factors responsible for CAPE are investigated further in order to physically interpret the observed behavior. CAPE for an undiluted air parcel is controlled in theory by surface air temperature, surface vapor mixing ratio, and air temperature as a function of height. The contribution of free-tropospheric moisture exists through the humidity term in virtual temperature but is very minor in magnitude compared to the other factors. Free-tropospheric humidity would be important when the entrainment of ambient dry air is taken into account but is not discussed in the present work.

The strategy here is to compute synthetic CAPE with the underlying parameters perturbed or fixed artificially. One of the parameters (e.g., $q_{v,s}$) is allowed to vary over time with all others fixed, and the parameter to be perturbed is switched from one experiment to another. In the "T_{BL} perturbed" experiment, for example, ABL temperature T_{BL} is as observed in the composite space while humidity and free-tropospheric temperature are fixed at the background level. Similarly, "$q_{v,s}$ perturbed" and "T_{FT} perturbed" experiments are conducted so that the impacts of surface moisture and free-tropospheric temperature T_{FT}, respectively, on CAPE are individually isolated. Here the ABL is defined as pressure levels at and below 925 hPa, and all other levels above are collectively considered as the free troposphere. The background level in the composite space is defined as the temporal average over the first and last 24 h combined in the same way as done earlier for computing anomaly fields. A control experiment is carried out with all the underlying parameters perturbed simultaneously.

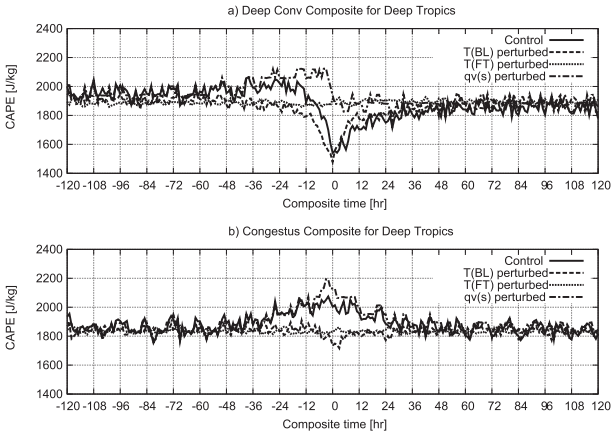

FIG. 8. The temporal sequence of synthetic CAPE (J kg^{-1}) composited with respect to (a) deep tropical deep convection and (b) deep tropical congestus. The control (solid), T_{BL} perturbed (dashed), T_{FT} perturbed (dotted), and $q_{v,s}$ perturbed (dotted–dashed) experiments are shown. See text for a detailed description of each experiment.

Figure 8 shows different experiments of synthetic CAPE. The control run reasonably captures the overall observed behavior, although it is not guaranteed to precisely reproduce the observations (Figs. 7c,f) because the synthetic CAPE is computed with the composite T and q_v instead of (as done for the observation) raw soundings to evaluate instantaneous CAPE before averaging. Other experiments are qualitatively different from the control. For the deep convection composite (Fig. 8a), the $q_{v,s}$ perturbed experiment shows no restoring phase following convection: the accumulated CAPE is quickly released out at the time when deep convection develops. The restoring phase is, as seen from the T_{BL} perturbed experiment, entirely ascribed to ABL temperature during the course of temperature recovery from the cool anomaly coincident with convection (Fig. 7b). The rapid drop of CAPE for half a day preceding convection, on the other hand, arises from the combined effects of ABL cooling and ventilation. The control run initially exhibits a subtle increase in CAPE closely following the $q_{v,s}$ perturbed run, but it begins to show a departure about 36 h before convection and then dramatically decreases until it eventually joins the T_{BL} perturbed experiment at $t = 0$.

The control experiment for the congestus composite (Fig. 8b) is entirely overlapped by the $q_{v,s}$ perturbed experiment except for a small deviation around $t = 0$. This deviation is presumably due to ABL temperature anomaly as suggested by a small dip in the T_{BL} perturbed experiment. It is inferred that the increase and decrease of CAPE associated with deep tropical congestus primarily result from the accumulation and dissipation of surface moisture, counteracted to a limited extent by ABL cooling.

In contrast to the $q_{v,s}$ and T_{BL} perturbed experiments, the T_{FT} perturbed experiment shows no evidence of modulating CAPE for either deep convection or congestus. The finding that the ABL temperature and moisture primarily control CAPE is consistent with earlier studies (Zhang 2003; Donner and Phillips 2003). It is noted that while the whole layer below 700 hPa containing both the ABL and lower free troposphere exhibits a coherent cool anomaly in association with deep convection (Fig. 7b), it is the ABL temperature that dominates CAPE.

d. Subtropics composite

Another composite analysis as performed for the deep tropics is applied to the three subtropical regions combined. The composite moisture fields shown in Fig. 9 clearly imply a free-tropospheric moistening associated with the convective development. The humidity modulation for deep convection (Figs. 9a–c) is even more outstanding than observed for the deep tropics (Figs. 6a–c) because the free troposphere in its background state is much drier in the subtropics. The moisture accumulation in the congestus composite is visible in the free-tropospheric relative humidity and vapor mixing ratio (Figs. 9d,e) but is as subtle as background diurnal modulation in CWV and $q_{v,s}$ (Fig. 9f).

The evolution of CAPE associated with subtropical deep convection (Fig. 10c) is quite different from the deep tropical case. CAPE slowly but drastically increases from the background level of about 300 J kg^{-1} until it reaches as high as 1000 J kg^{-1}, and then gradually decays back to the background level. Deep convective rainfall sharply rises and falls within ± 12 h (Fig. 10c), accompanied by a momentary destabilization of the atmosphere as inferred from $\theta_{e,s} - \theta_e^*$ (Fig. 10a). The evolution of CAPE, somewhat analogous to the deep tropical congestus case but having a much larger amplitude, extends well beyond the duration of rainfall, and hence moist convection is more of a passive response than an adjusting force to the large-scale environment. The composite temperature exhibits a striking cool anomaly in the free troposphere lasting 5 days from -60 through $+60$ h (Fig. 10b). A weaker but persistent cool anomaly is also observed in association with congestus (Fig. 10e). CAPE hardly varies with the congestus development (Fig. 10f).

Two caveats need to be mentioned. First, the frequency of deep convective occurrence is only 0.16% in the subtropics, more than 20 times lower than in the deep tropics (Table 1). The drastic moistening of the free troposphere as seen above does occur from time to

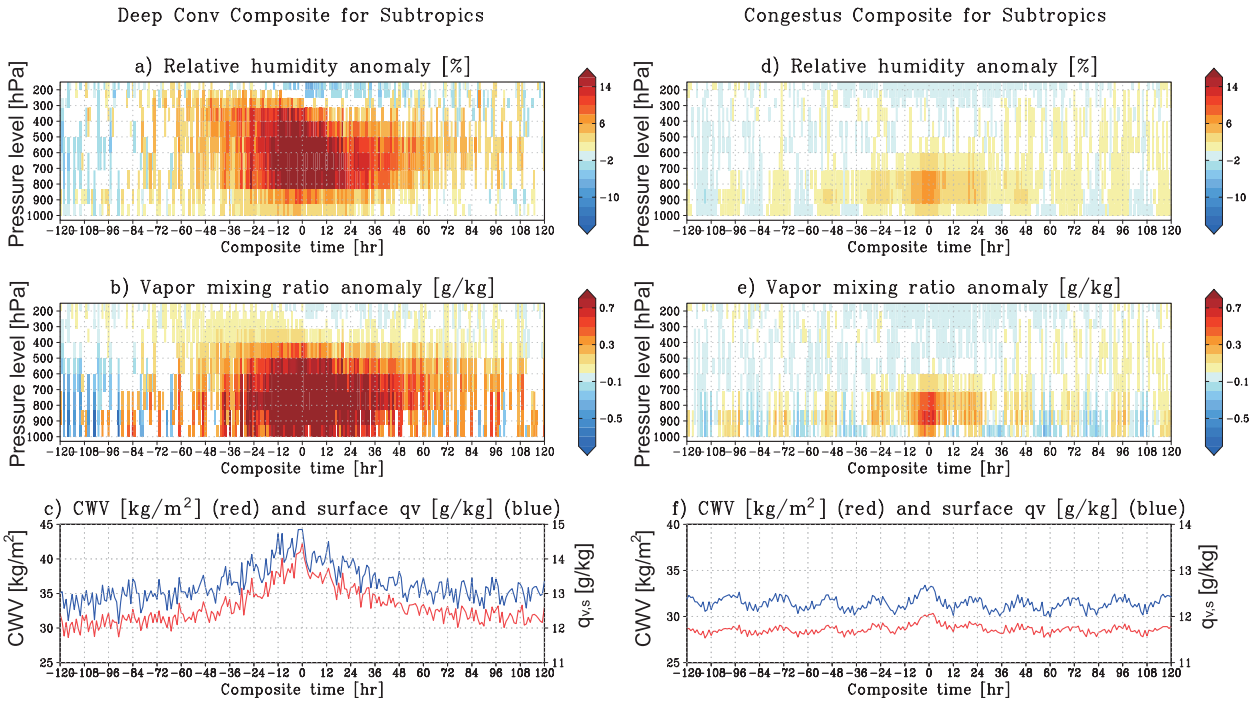

FIG. 9. As in Fig. 6, but for the subtropics.

time but probably not so frequently as to exert a significant long-term influence on the environment. Second, the evolution of subtropical CAPE as seen in Fig. 10 requires a careful interpretation. CAPE appears to start increasing as early as 36 h before deep convection develops, while it is not until −12 h that $\theta_{e,s} - \theta_e^*$ gains a positive section in the middle troposphere so LFC is definable. Given that CAPE must vanish when LFC is indefinable, the gradual enhancement of CAPE for $t <$ −12 h does not necessarily imply a continuous destabilization on an event-by-event basis. The percentage of unstable sounding or nonzero CAPE is depicted as a function of composite time in Fig. 11a. The percentage is consistently higher than 95% in the deep tropics, indicating that deep tropical soundings stay unstable most of the time. The deep tropical composite therefore consists of a relatively homogeneous set of soundings having a finite CAPE. In the subtropics, on the other hand, the percentage of nonzero CAPE is much lower and varies over time in a way similar to the composite CAPE itself shown in Fig. 10. The subtropical CAPE composited exclusively from unstable soundings (Fig. 11b) indeed exhibits a similar evolution to Fig. 10c but with somewhat higher values overall. The composite subtropical CAPE should be thus interpreted to some extent as a stochastic ensemble of zero and nonzero CAPEs with their relative fractions changing with time, unlike the deep tropics case where CAPE is finite most of the time.

5. Summary and discussion

The large-scale forcing and response of tropical and subtropical atmospheres to moist convection are explored in this paper. The main goal is to provide an observational assessment of the key assumption underlying the QE hypothesis that convective adjustment takes place quickly and efficiently. To this end, TRMM and *Aqua* satellite data are analyzed together to study the evolution of composite temperature and humidity fields on an hourly basis before and after convection occurs, exploiting the fact that the temporal interval between the TRMM and *Aqua* overpasses changes from one orbit to another.

In the deep tropics, a systematic moisture transport from the ABL to the free troposphere is clearly observed in association with deep convection. The vertical moisture transport is likely to be promoted by the ABL ventilation due to deep convection when it occurs, while free-tropospheric moistening begins somewhat earlier than the deep convective development. The latter fact appears to be consistent with another picture, namely that free-tropospheric humidity exerts a strong control on the onset of precipitation, as discussed in the literature (e.g., Sherwood 1999; Raymond 2000; Bretherton et al. 2004; Raymond et al. 2007). When the effect of ABL moisture is singled out among the factors controlling CAPE (i.e., the $q_{v,s}$ perturbed experiment),

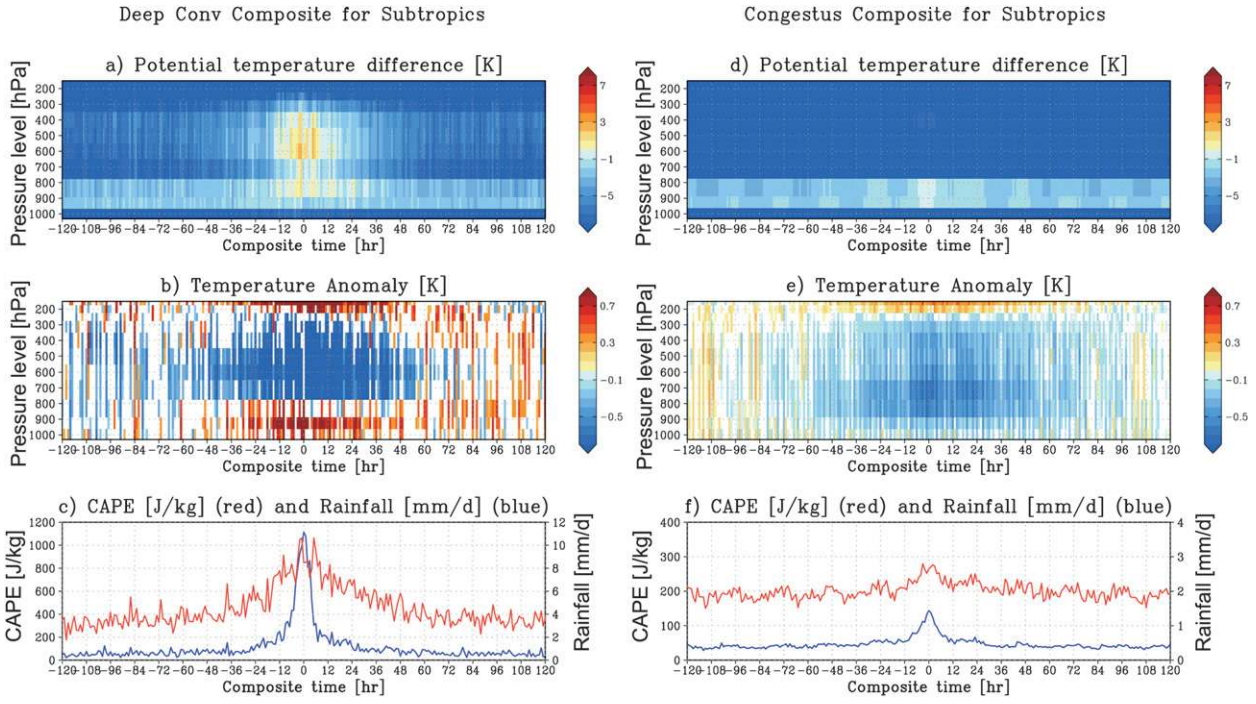

FIG. 10. As in Fig. 7, but for the subtropics.

CAPE is found to steadily accumulate as the ABL gradually moistens until it drops back sharply (for a few hours) at the time when the ABL is abruptly ventilated. The quick ABL ventilation suggests a swift convective adjustment in action, while the prior accumulation of CAPE does not imply continuous adjustment to equilibrium.

The actual evolution of CAPE exhibits a somewhat unexpected behavior as ABL temperature comes into play. A cool anomaly that emerges in the ABL and lower troposphere grows over a short period of time (~12 h) as deep convection develops. This cool anomaly reduces CAPE, and a restoring phase of CAPE follows as the cool anomaly diminishes after deep convection shuts off. A plausible origin of the lower-tropospheric (including ABL) cooling is the adiabatic cooling due to a large-scale ascent, perhaps augmented by the evaporative cooling in stratiform rain. One might expect that, in the mid- to upper troposphere, large-scale adiabatic cooling can be offset by convective heating (or apparent heating, Q_1), when the Q_1 profile is top-heavy as is typical for tropical organized convective systems (Yanai et al. 1973; Houze 1982; Johnson 1984). A corresponding warm anomaly is indeed observed in the 700–300-hPa layer in synchronization with the lower-tropospheric cooling. Raymond and Sessions (2007) argued, based on local moist entropy budget, that such a bipolar temperature anomaly would have an effect of intensifying rainfall.

It is tempting to speculate that this thermodynamic response of the atmosphere might serve as a forcing mechanism for inertio-gravity waves of a relevant oscillatory period. Given that the temperature anomaly lasts approximately ±12 h around the deep convective occurrence, a 2-day mode would be preferentially excited.

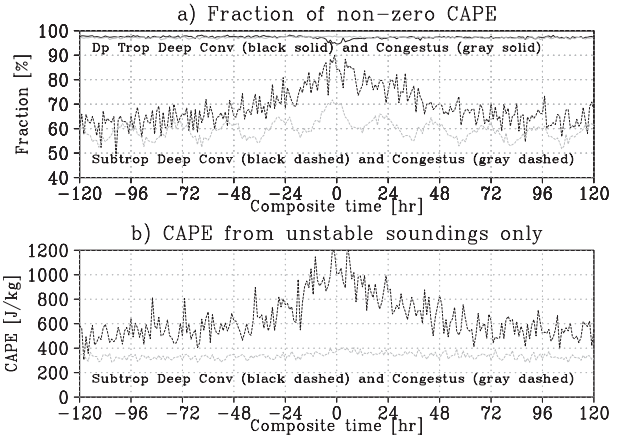

FIG. 11. (a) The percentage of unstable sounding (CAPE > 0) sampled for the composite plot: deep tropical deep convection (black solid), deep tropical congestus (gray solid), subtropical deep convection (black dashed), and subtropical congestus (gray dashed). (b) Subtropical CAPE composited exclusively from unstable soundings for deep convection (black dashed) and congestus (gray dashed).

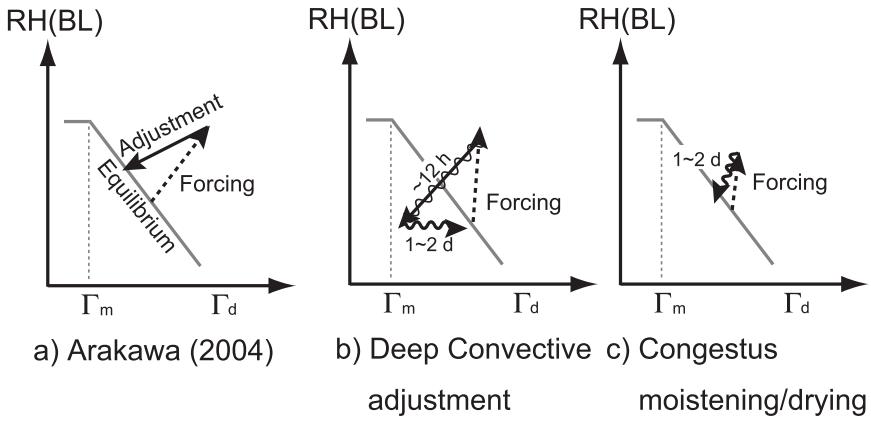

FIG. 12. Schematic of large-scale forcing and convective adjustment in terms of tropospheric temperature lapse rate (abscissa) and ABL relative humidity (ordinate) as devised by Arakawa (2004). Dashed arrow denotes large-scale forcing, solid arrow is convective adjustment, and wavy arrow represents large-scale response. The gray line represents the equilibrium solution. (a) Original QE hypothesis illustrated by Arakawa (2004). (b) As inferred from the present analysis for the deep tropics. A large-scale response coincides with convective adjustment where the solid and wavy arrows are superposed together, in which case the time scale is limited by the (slower) large-scale response (~12 h). (c) As in (b), but for congestus instead of deep convection.

The quasi-2-day wave documented in the literature (Takayabu et al. 1996; Haertel and Johnson 1998; Haertel and Kiladis 2004) is actually known to exhibit a similar temperature structure in its peak phase. Haertel et al. (2008) showed that a temperature dipole in the 2-day wave is accounted for by the second and third vertical mode projection of convective heating, which is considered to be excited by stratiform and congestus precipitation. The lower-tropospheric cooling should be dynamically connected with the stratiform cooling in order for convectively coupled waves to survive moist convective damping (Mapes 2000). The effects of convective heating from various types of clouds will be explored in future work in relevance to the equatorial wave dynamics.

The evolution of CAPE associated with deep tropical congestus is essentially different from the deep convective case outlined above. CAPE slowly increases with time as ABL moisture accumulates over a period of about 24–48 h until congestus clouds develop, and then decays as slowly back to the initial level. Neggers et al. (2007) argued that shallow cumulus typically takes about 10^5 s to ventilate the ABL, consistent with the current result inferred from the congestus composite. Temperature perturbation is so subtle in the congestus case that ABL moisture is almost solely responsible for the CAPE variability. Congestus enhances the free-tropospheric humidity to some extent, although the moistening effect is less pronounced in both magnitude and depth compared to the deep convective case.

Present findings are summarized below in the context of the large-scale processes and convective adjustment in the deep tropics. Among a variety of different QE formulations considered to date, a schematic representation devised by Arakawa (2004) is adopted here as the test bed, where the atmospheric state is described in terms of boundary layer humidity and tropospheric temperature lapse rate (Fig. 12). This particular representation is meant to address a range of QE versions including the earliest formulation by Arakawa and Schubert (1974) and some influential QE variants as explored by Betts (1986) and Emanuel et al. (1994). The original QE hypothesis (Fig. 12a) postulates that a departure from the equilibrium state forced by large-scale processes is immediately pulled back to equilibrium by convective adjustment. The observation (Fig. 12b), on the other hand, implies that a quick reduction of ABL humidity (ordinate) is concurrent with a relatively slow (~12 h) decline of the ABL temperature. This ABL cooling is linked with the atmospheric response comprising a lower-tropospheric cooling and upper-tropospheric warming, leading to a momentary decrease in temperature lapse rate (abscissa in Fig. 12). The lapse rate decrease temporarily makes the atmosphere enter the stable regime across the equilibrium line, while an equilibrium state is restored within a day or two as the lapse rate anomaly disappears. As such, the atmosphere acts somewhat like a damping oscillation rather than a monotonic damping. The idealized forms of the QE hypothesis in which the whole troposphere instantly (or within a few hours at most) adjusts itself toward an equilibrium state are not fully supported by the observation.

The congestus development accompanies systematic prior moistening and subsequent drying. These processes take place over a period of 24 h or even longer (Fig. 12c), while congestus rainfall shuts off within about 12 h. The ABL drying process is not a swift ventilation as found for deep convective but persists long after convection stops working. It is thus less clear than in the deep convective case that rapid convective adjustment is at work in association with congestus clouds. The QE hypothesis would again not offer a valid closure principle during times when moist convection is driven by congestus alone.

There are schools of QE thinking that are not conceptualized by Fig. 12. The most notable among them is the boundary layer quasi-equilibrium (BLQ), where surface heat fluxes are assumed to be thermodynamically in balance with convective downdraft (Raymond 1995; Emanuel 1995). BLQ places no explicit constraint on the free troposphere, so that the anomalous behavior of temperature lapse rate (Fig. 12b) does not rule out BLQ. The current composite analysis, however, shows a prior buildup of ABL moisture and an ABL cooling persisting for a day or two after convection ceases, not precisely in line with BLQ that has been argued to hold on time scales of 1/2–1 day (Raymond 1995). A further assessment of BLQ requires a careful heat budget analysis involving surface fluxes and convective downdraft and should be done elsewhere.

The atmosphere is climatologically so stable in the subtropics that conditional neutrality as presupposed by the QE hypothesis is scarcely achieved. Deep convection in the subtropical regions is less frequent by an order of magnitude than in the deep tropics and incapable of retaining moist neutrality against stabilizing large-scale forcings. In rare occasions when deep convection occurs, however, the subtropical atmosphere is destabilized for a short period of time (~24 h), preceded by the (stochastic) accumulation of CAPE and succeeded by the dissipation. This behavior implies no sign of convective adjustment. It is found that a free-tropospheric cool anomaly persists for a period well beyond the duration of rainfall when convection occurs in the subtropics. Origins of the persistent cool anomaly are unknown, while it possibly suggests that external disturbances such as upper-tropospheric troughs may often accompany the deep convective development in the subtropics. Subtropical deep convection is perhaps more of a passive player responding to large-scale forcings than a key ingredient actively controlling the atmospheric thermodynamics.

The present paper, as the first attempt to apply a new composite analysis method to TRMM and *Aqua* measurements, is focused intentionally on contrasting extreme cases of deep convection and congestus. In reality, the spectrum of tropical convective clouds is quite rich and variable, having different types of clouds mixed together with different proportions. Major modes of the tropical oscillations including the MJO are known to accompany a systematic shift in the convective cloud spectrum from the shallow cumulus dominated phase to the deep convective stage (e.g., Mapes et al. 2006), which can be crucial for dynamically driving and maintaining the waves (Khouider and Majda 2006; Kuang 2008; Haertel et al. 2008). The role of convective adjustment potentially changes in the course of the oscillation and, if so, the phase dependence of convective adjustment time might deserve attention as an element of the tropical wave dynamics. This study is also confined to the regions well representative of either the deep tropics or subtropics. There are border regions of their own climatological importance located in between the deep tropics and subtropics (Lintner and Neelin 2007). Future work on the lines of the present analysis will be extended beyond the current scope in hopes to offer a broader perspective on how the large-scale dynamics interact with convective clouds.

Acknowledgments. The author thanks Dave Raymond, Jim Benedict, and an anonymous reviewer for their insightful comments and helpful suggestions. The TRMM PR (2A25) and VIRS (1B01) datasets were provided by the Japan Aerospace Exploration Agency (JAXA) Earth Observation Research Center (EORC). The AIRS/AMSU level-3 daily gridded product was acquired as part of the activities of NASA's Science Mission Directorate and is archived and distributed by the Goddard Earth Sciences (GES) Data and Information Services Center (DISC). The daily gridded AMSR-E precipitation product was obtained from Colorado State University (rain.atmos.colostate.edu/RAINMAP/). The author is grateful to Hiroki Ichikawa for his assistance to download the AIRS dataset. This work is supported by the Ministry of Education, Culture, Sports, Science, and Technology (MEXT) Grant-in-Aid for Young Scientists (Grant 20740269).

APPENDIX A

Estimation of Surface Vapor Mixing Ratio

The lowest-level humidity available in the AIRS product is the layer mean within 1000–925 hPa; it generally does not substitute for $q_{v,s}$ as it is. The lowermost AIRS humidity is thus extrapolated down to the surface using a simplified lower-ABL model (Fig. A1). The model is based on the following assumptions so it conceptually

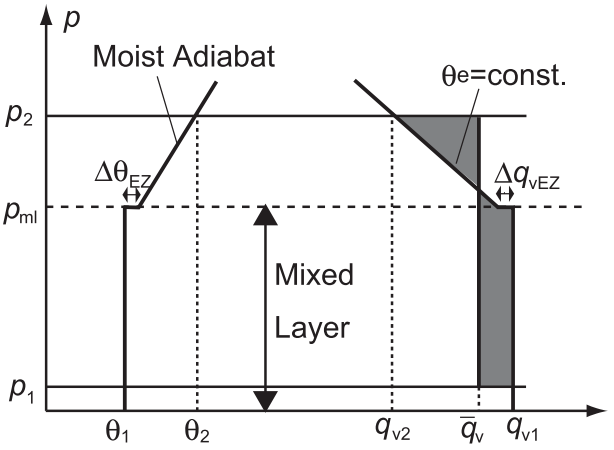

FIG. A1. Schematic of the lower ABL model used for estimating $q_{v,s}$. Shade indicates the area to be integrated in (A3).

represents the cloud-topped ABL typical over tropical and subtropical oceans (e.g., Malkus 1958): 1) The layer bounded by $p_1 = 1000$ hPa and $p_2 = 925$ hPa is considered to be a sublayer of the ABL. The subscripts 1 and 2 hereafter denote these two levels. The temperature inversion, if exists, is assumed to lie above p_2 and does not affect the present discussion. 2) Air temperatures at p_1 and p_2 and the vapor mixing ratio averaged between these levels $\overline{q_v}$ are known from AIRS observations. 3) Potential temperature θ is vertically constant within the mixed layer while $\theta(p)$ follows the moist adiabat above. 4) Vapor mixing ratio is vertically homogeneous within the mixed layer, while it decreases with height above so that θ_e is conserved. 5) The entrainment zone (or transition layer) is an infinitely thin layer with a prescribed discontinuity in θ and q_v, denoted by $\Delta\theta_{\rm EZ}$ and $\Delta q_{v\rm EZ}$, at the mixed layer top.

The overall procedure to obtain $q_{v,s}$ proceeds as follows. The mixed layer top level $p_{\rm ml}$ is first determined from the observed T_1 and T_2 (or θ_1 and θ_2). This is simply done by finding the level where $\theta(p)$ extending down moist adiabatically from θ_2 meets the value at the mixed layer top, that is,

$$\theta_1 + \Delta\theta_{\rm EZ} = \theta_2 + \left(\frac{d\theta}{dp}\right)_{\rm MA}(p_{\rm ml} - p_2), \quad \text{(A1)}$$

where

$$\left(\frac{d\theta}{dp}\right)_{\rm MA} = -\frac{\theta}{p}\frac{R}{C_p}\left(1 - \frac{1 + q_s L/RT}{1 + q_s L^2/R_v C_p T^2}\right).$$

The vertical distribution of vapor mixing ratio is next obtained for levels between $p_{\rm ml}$ and p_2 as

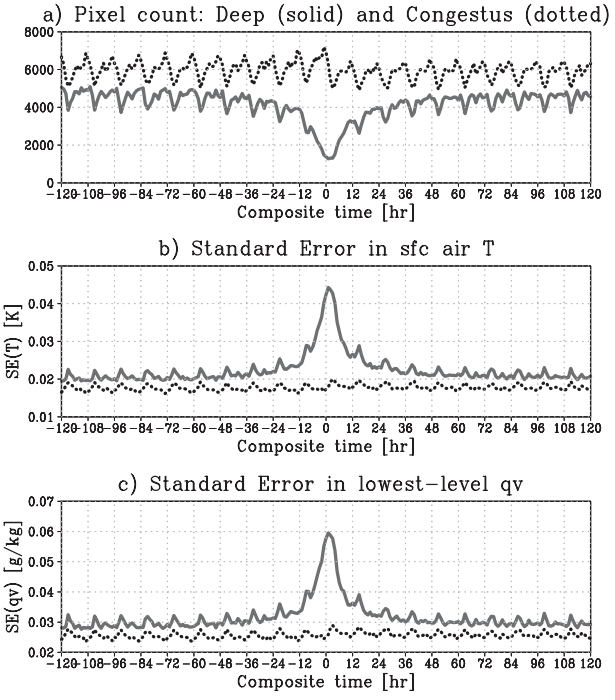

FIG. B1. The temporal sequence of (a) observed pixel count (i.e., sample size for each composite time bin), (b) standard error in surface air temperature, and (c) standard error in lowest-level q_v (1000–925-hPa mean), all composited with respect to deep tropical deep convection (solid) and congestus (dotted).

$$q_v(p) = \frac{C_p T(p)}{L}\ln\left[\frac{\theta_2}{\theta(p)}\right] + \frac{T(p)}{T_2}q_{v,2}, \quad \text{(A2)}$$

where C_p and L are the specific heat of dry air at constant pressure and specific latent heat, respectively, and $\theta(p)$ and $T(p)$ follow the moist adiabat. Finally, $q_{v,1}$ as a proxy of $q_{v,s}$ is determined so that the vertically averaged vapor mixing ratio equals the observed $\overline{q_v}$, that is,

$$\int_{p_2}^{p_1}[q_v(p) - \overline{q_v}]\,dp = 0. \quad \text{(A3)}$$

This integral equation is solved iteratively until the optimal solution of $q_{v,1}$ is obtained.

Currently $\Delta\theta_{\rm EZ}$ is prescribed to be 1 K (e.g., Betts 1973) and $\Delta q_{v\rm EZ}$ to be 3 g kg^{-1} (cf. Fig. 3 of Johnson et al. 2001). These parameters are by no means universally constant and would require a more flexible characterization for the precise evaluation of $q_{v,s}$. The present study, however, adopts those fixed numbers for $\Delta\theta_{\rm EZ}$ and $\Delta q_{v\rm EZ}$ since they suffice to capture the overall structure of the composite $q_{v,s}$ and CAPE.

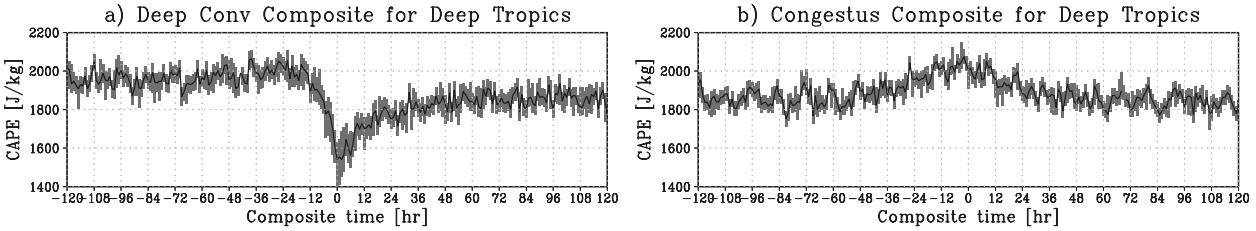

FIG. B2. Uncertainty in the composite CAPE for (a) deep convection and (b) congestus in the deep tropics. Error bars correspond to twice the standard error in T_s and $q_{v,s}$.

APPENDIX B

On the Accuracy of the Composite AIRS Parameters

AIRS temperature and humidity measurements are affected by clouds and need a careful error estimate when applied to cloudy scenes. As shown in Fig. B1a, the number of AIRS observations $N(t)$ drops in the vicinity of $t = 0$ when composited with respect to deep convection since a significant fraction of AIRS observations are screened out by quality control within a heavily precipitating $1° \times 1°$ pixel. Such sampling loss is not appreciable in the congestus composite. Periodic spikes spaced every 12 h imply that the sampling inhomogeneity specific to the TRMM and *Aqua* orbital configurations has not been completely smoothed out in the composite space.

Figures B1b and B1c show the standard error of AIRS surface temperature T_s and lowest-level vapor mixing ratio, respectively, in the composite space. The standard error, a measure often used for testing the sample mean against the true mean, is computed as the mean of the rms error associated with individual estimates divided by the square root of N. The lowest level available has been selected because it tends to have larger errors than any higher levels. The present analysis ingests instantaneous error estimates provided in the AIRS data products, so that local weather conditions affecting the retrieval accuracy are taken into account on a scene-by-scene basis. The standard error is peaked at $t = 0$ for the deep convective case, primarily because of the inverse proportionality to $\sqrt{N}$. The standard error reaches 0.045 K for temperature and 0.06 g kg^{-1} for vapor mixing ratio at worst. These values stay smaller than the variability of interest in the composite plot.

The uncertainties in ABL temperature and moisture are a main source of error in the CAPE estimate. Figure B2 shows the CAPE uncertainty in the composite space, where error bars are calculated with T_s and $q_{v,s}$ perturbed by twice the standard error away from the mean. The magnitude of uncertainty is not so large as to obscure the overall behavior of the composite CAPE, and thus the main conclusions of this work are insensitive to errors originating from the temperature and humidity sounding data.

REFERENCES

Arakawa, A., 2004: The cumulus parameterization problem: Past, present, and future. *J. Climate,* **17,** 2493–2525.

——, and W. H. Schubert, 1974: Interaction of a cumulus cloud ensemble with the large-scale environment, Part I. *J. Atmos. Sci.,* **31,** 674–701.

Aumann, H. H., and Coauthors, 2003: AIRS/AMSU/HSB on the *Aqua* mission: Design, science objectives, data products, and processing systems. *IEEE Trans. Geosci. Remote Sens.,* **41,** 253–264.

Benedict, J. J., and D. A. Randall, 2007: Observed characteristics of the MJO relative to maximum rainfall. *J. Atmos. Sci.,* **64,** 2332–2354.

Betts, A. K., 1973: Non-precipitating cumulus convection and its parameterization. *Quart. J. Roy. Meteor. Soc.,* **99,** 178–196.

——, 1986: A new convective adjustment scheme. Part I: Observational and theoretical basis. *Quart. J. Roy. Meteor. Soc.,* **112,** 677–691.

——, and M. J. Miller, 1986: A new convective adjustment scheme. Part II: Single column tests using GATE wave, BOMEX, ATEX and arctic air-mass data sets. *Quart. J. Roy. Meteor. Soc.,* **112,** 693–709.

Bretherton, C. S., M. E. Peters, and L. E. Back, 2004: Relationships between water vapor path and precipitation over the tropical oceans. *J. Climate,* **17,** 1517–1528.

Brown, R. G., and C. S. Bretherton, 1997: A test of the strict quasi-equilibrium theory on long time and space scales. *J. Atmos. Sci.,* **54,** 624–638.

Donner, L. J., and V. T. Phillips, 2003: Boundary layer control on convective available potential energy: Implications for cumulus parameterization. *J. Geophys. Res.,* **108,** 4701, doi:10.1029/2003JD003773.

Emanuel, K. A., 1993: The effect of convective response time on WISHE models. *J. Atmos. Sci.,* **50,** 1763–1775.

——, 1995: The behavior of a simple hurricane model using a convective scheme based on subcloud-layer entropy equilibrium. *J. Atmos. Sci.,* **52,** 3960–3968.

——, J. D. Neelin, and C. S. Bretherton, 1994: On large-scale circulations in convecting atmospheres. *Quart. J. Roy. Meteor. Soc.,* **120,** 1111–1143.

Haertel, P. T., and R. H. Johnson, 1998: Two-day disturbances in the equatorial western Pacific. *Quart. J. Roy. Meteor. Soc.,* **124,** 615–636.

——, and G. N. Kiladis, 2004: Dynamics of 2-day equatorial waves. *J. Atmos. Sci.,* **61,** 2707–2721.

——, ——, A. Denno, and T. M. Rickenbach, 2008: Vertical-mode decompositions of 2-day waves and the Madden–Julian oscillation. *J. Atmos. Sci.,* **65,** 813–833.

Holloway, C. E., and J. D. Neelin, 2007: The convective cold top and quasi equilibrium. *J. Atmos. Sci.,* **64,** 1467–1487.

Houze, R. A., Jr., 1982: Cloud clusters and large-scale vertical motions in the tropics. *J. Meteor. Soc. Japan,* **60,** 396–410.

Johnson, R. H., 1984: Partitioning tropical heat and moisture budgets into cumulus and mesoscale components: Implications for cumulus parameterization. *Mon. Wea. Rev.,* **112,** 1590–1601.

——, T. M. Rickenbach, S. A. Rutledge, P. E. Ciesielski, and W. H. Schubert, 1999: Trimodal characteristics of tropical convection. *J. Climate,* **12,** 2397–2418.

——, P. E. Ciesielski, and J. A. Cotturone, 2001: Multiscale variability of the atmospheric mixed layer over the western Pacific warm pool. *J. Atmos. Sci.,* **58,** 2729–2750.

Katsumata, M., R. H. Johnson, and P. E. Ciesielski, 2009: Observed synoptic-scale variability during the developing phase of an ISO over the Indian Ocean during MISMO. *J. Atmos. Sci.,* **66,** 3434–3448.

Kemball-Cook, S. R., and B. C. Weare, 2001: The onset of convection in the Madden–Julian oscillation. *J. Climate,* **14,** 780–793.

Khouider, B., and A. J. Majda, 2006: A simple multicloud parameterization for convectively coupled tropical waves. Part I: Linear analysis. *J. Atmos. Sci.,* **63,** 1308–1323.

Kikuchi, K., and Y. N. Takayabu, 2004: The development of organized convection associated with the MJO during TOGA COARE IOP: Trimodal characteristics. *Geophys. Res. Lett.,* **31,** L10101, doi:10.1029/2004GL019601.

Kiladis, G. N., K. H. Straub, and P. T. Haertel, 2005: Zonal and vertical structure of the Madden–Julian oscillation. *J. Atmos. Sci.,* **62,** 2790–2809.

Kondo, Y., A. Higuchi, and K. Nakamura, 2006: Small-scale cloud activity over the Maritime Continent and the western Pacific as revealed by satellite data. *Mon. Wea. Rev.,* **134,** 1581–1599.

Kuang, Z., 2008: A moisture-stratiform instability for convectively coupled waves. *J. Atmos. Sci.,* **65,** 834–854.

Kummerow, C. D., W. Barnes, T. Kozu, J. Shiue, and J. Simpson, 1998: The Tropical Rainfall Measuring Mission (TRMM) sensor package. *J. Atmos. Oceanic Technol.,* **15,** 809–817.

——, and Coauthors, 2001: The evolution of the Goddard Profiling Algorithm (GPROF) for rainfall estimation from passive microwave sensors. *J. Appl. Meteor.,* **40,** 1801–1820.

Lintner, B. R., and J. D. Neelin, 2007: A prototype for convective margin shifts. *Geophys. Res. Lett.,* **34,** L05812, doi:10.1029/2006GL027305.

Lord, S. J., 1982: Interaction of a cumulus cloud ensemble with the large-scale environment. Part III: Semi-prognostic test of the Arakawa–Schubert cumulus parameterization. *J. Atmos. Sci.,* **39,** 88–103.

——, and A. Arakawa, 1980: Interaction of a cumulus cloud ensemble with the large-scale environment. Part II. *J. Atmos. Sci.,* **37,** 2677–2692.

Malkus, J. S., 1958: On the structure of the trade wind moist layer. *Pap. Phys. Oceanogr. Meteor.,* **13,** 1–47.

Mapes, B., 2000: Convective inhibition, subgrid-scale triggering energy, and stratiform instability in a toy tropical wave model. *J. Atmos. Sci.,* **57,** 1515–1535.

——, S. Tulich, J. Lin, and P. Zuidema, 2006: The mesoscale convection life cycle: Building block or prototype for large-scale tropical waves? *Dyn. Atmos. Oceans,* **42,** 3–29.

——, R. Milliff, and J. Morzel, 2009: Composite life cycle of maritime tropical mesoscale convective systems in scatterometer and microwave satellite observations. *J. Atmos. Sci.,* **66,** 199–208.

Masunaga, H., 2009: A 9-season observation TRMM observation of the austral summer MJO and low-frequency equatorial waves. *J. Meteor. Soc. Japan,* **87A,** 295–315.

——, and C. D. Kummerow, 2006: Observations of tropical precipitating clouds ranging from shallow to deep convective systems. *Geophys. Res. Lett.,* **33,** L16805, doi:10.1029/2006GL026547.

——, T. S. L'Ecuyer, and C. D. Kummerow, 2005: Variability in the characteristics of precipitation systems in the tropical Pacific. Part I: Spatial structure. *J. Climate,* **18,** 823–840.

——, ——, and ——, 2006: The Madden–Julian oscillation recorded in early observations from the Tropical Rainfall Measuring Mission (TRMM). *J. Atmos. Sci.,* **63,** 2777–2794.

Moorthi, S., and M. J. Suarez, 1992: Relaxed Arakawa–Schubert: A parameterization of moist convection for general circulation models. *Mon. Wea. Rev.,* **120,** 978–1002.

Neelin, J. D., and J.-Y. Yu, 1994: Modes of tropical variability under convective adjustment and the Madden–Julian oscillation. Part I: Analytical theory. *J. Atmos. Sci.,* **51,** 1876–1894.

——, and N. Zeng, 2000: A quasi-equilibrium tropical circulation model—Formulation. *J. Atmos. Sci.,* **57,** 1741–1766.

——, O. Peters, J.W.-B. Lin, K. Hales, and C. E. Holloway, 2008: Rethinking convective quasi-equilibrium: Observational constraints for stochastic convective schemes in climate models. *Philos. Trans. Roy. Soc. London,* **366A,** 2581–2602, doi:10.1098/rsta.2008.0056.

Neggers, R. A. J., J. D. Neelin, and B. Stevens, 2007: Impact mechanisms of shallow cumulus convection on tropical climate dynamics. *J. Climate,* **20,** 2623–2642.

Raymond, D. J., 1995: Regulation of moist convection over the west Pacific warm pool. *J. Atmos. Sci.,* **52,** 3945–3959.

——, 2000: Thermodynamic control on tropical rainfall. *Quart. J. Roy. Meteor. Soc.,* **126,** 889–898.

——, and S. L. Sessions, 2007: Evolution of convection during tropical cyclogenesis. *Geophys. Res. Lett.,* **34,** L06811, doi:10.1029/2006GL028607.

——, ——, and Ž. Fuchs, 2007: A theory for the spinup of tropical depressions. *Quart. J. Roy. Meteor. Soc.,* **133,** 1743–1754.

Reed, R. J., and E. E. Recker, 1971: Structure and properties of synoptic-scale wave disturbances in the equatorial western Pacific. *J. Atmos. Sci.,* **28,** 1117–1133.

Sherwood, S. C., 1999: Convective precursors and predictability in the tropical western Pacific. *Mon. Wea. Rev.,* **127,** 2977–2991.

——, and R. Wahrlich, 1999: Observed evolution of tropical deep convective events and their environment. *Mon. Wea. Rev.,* **127,** 1777–1795.

Susskind, J., C. D. Barnet, and J. M. Blaisdell, 2003: Retrieval of atmospheric and surface parameters from AIRS/AMSU/HSB data in the presence of clouds. *IEEE Trans. Geosci. Remote Sens.,* **41,** 390–409.

——, ——, ——, L. Iredell, F. Keita, L. Kouvaris, G. Molnar, and M. Chahine, 2006: Accuracy of geophysical parameters derived from Atmospheric Infrared Sounder/Advanced Microwave Sounding unit as a function of fractional cloud cover. *J. Geophys. Res.,* **111,** D09S17, doi:10.1029/2005JD006272.

Takayabu, Y. N., K.-M. Lau, and C.-S. Sui, 1996: Observation of a quasi-2-day wave during TOGA COARE. *Mon. Wea. Rev.,* **124,** 1892–1913.

Xu, K.-M., and K. A. Emanuel, 1989: Is the tropical atmosphere conditionally unstable? *Mon. Wea. Rev.,* **117,** 1471–1479.

——, A. Arakawa, and S. K. Krueger, 1992: The macroscopic behavior of cumulus ensembles simulated by a cumulus ensemble model. *J. Atmos. Sci.,* **49,** 2402–2420.

Yanai, M., S. Esbensen, and J.-H. Chu, 1973: Determination of bulk properties of tropical cloud clusters from large-scale heat and moisture budgets. *J. Atmos. Sci.,* **30,** 611–627.

Zelinka, M. D., and D. L. Hartmann, 2009: Response of humidity and clouds to tropical deep convection. *J. Climate,* **22,** 2389–2404.

Zhang, G. J., 2003: Convective quasi-equilibrium in the tropical western Pacific: Comparison with midlatitude continental environment. *J. Geophys. Res.,* **108,** 4592, doi:10.1029/2003JD003520.

——, 2009: Effects of entrainment on convective available potential energy and closure assumptions in convection parameterization. *J. Geophys. Res.,* **114,** D07109, doi:10.1029/2008JD010976.

——, and N. A. McFarlane, 1995: Sensitivity of climate simulations to the parameterization of cumulus convection in the Canadian Climate Center general circulation model. *Atmos.–Ocean,* **33,** 407–446.